Journal of Alloys and Compounds 510 (2012) 46–53

Contents lists available at ScienceDirect

Journal of Alloys and Compounds

journal homepage: www.elsevier.com/locate/jallcom

Analysis of grain growth process in melt spun Fe–B alloys under the initial saturated grain boundary segregation condition

Z. Chen [a,b,*], F. Liu [b], X.Q. Yang [c], Y. Fan [a], C.J. Shen [a]

[a] School of Material Science and Engineering, China University of Mining and Technology, Xuzhou, Jiangsu 221008, PR China
[b] State Key Laboratory of Solidification Processing, Northwestern Polytechnical University, Xi'an, Shaanxi 710072, China
[c] School of Chemical Engineering and Technology, China University of Mining and Technology, Xuzhou, Jiangsu 221008, PR China

ARTICLE INFO

Article history:
Received 20 April 2011
Received in revised form 9 August 2011
Accepted 10 August 2011
Available online 19 August 2011

Keywords:
Grain growth
Thermal stability
Fe–B alloys
Grain boundary segregation

ABSTRACT

A grain growth process in the melt spun low-solid-solubility Fe–B alloys was analyzed under the initial saturated grain boundary (GB) segregation condition. Applying melt spinning technique, single-phase supersaturated nanograins were prepared. Grain growth behavior of the single-phase supersaturated nanograins was investigated by performing isothermal annealing at 700 °C. Combined with the effect of GB segregation on the initial GB excess amount, the thermo-kinetic model [Chen et al., Acta Mater. 57 (2009) 1466] was extended to describe the initial GB segregation condition of nanoscale Fe–B alloys. In comparison of pure kinetic model, pure thermodynamic model and the extended thermo-kinetic model, an initial saturated GB segregation condition was determined. The controlled-mechanism of grain growth under initial saturated GB segregation condition was proposed using two characteristic annealing times (t_1 and t_2), which included a mainly kinetic-controlled process ($t \le t_1$), a transition from kinetic-mechanism to thermodynamic-mechanism ($t_1 < t < t_2$) and pure thermodynamic-controlled process ($t \ge t_2$).

1. Introduction

The melt spinning technique allows the rapid solidification of metallic alloys to produce amorphous or nanocrystalline (NC) materials [1–3]. NC ribbons of Fe-based alloys, such as Fe–B, Fe–Si–B–P–Cu, Fe–Cu–Mo–Si–B have been proved to possess excellent soft magnetic properties because of the reduction of grain size [4,5]. Analogously, Liu et al. reviewed that the new rare earth–Mg–Ni-based hydrogen storage alloys with small crystal grains were usually prepared by rapid quenching and melt spinning [6], since the reduction of grain size upon melt spinning obviously enhances the cyclic stability of the alloy electrodes.

However, the melt spinning technique is a non-equilibrium solidification which changes the growth velocity and solidification behavior [4,7,8], so that the melt-spun alloys are unstable because of the non-equilibrium effects. For nanoscale alloys, the thermal stability is crucial to engineering applications. Therefore, an understanding of the thermal stability is scientifically and technologically important.

Stability of the as-prepared alloys with respect to grain growth was discussed controversially. Some authors claimed that solute drag (i.e., kinetic effect) by alloy or impurity atoms reduced the mobility of the grain boundaries (GBs) [9–11] whereas others attributed it to a vanishing GB energy σ_b (i.e., thermodynamic effect) [12,13]. However, the stabilized grain size cannot be determined by the kinetic models, and the evolution of grain size cannot be described by the thermodynamic approaches [14]. According to Zhang et al. [15], nanoscale grain growth belongs to a kinetic process controlled by thermodynamic factor (reduced σ_b with grain growth). Therefore, the thermo-kinetic model which considers the mixed effect of kinetics and thermodynamics is more appropriate for describing the process of grain growth. Liu et al. [16] first attempted to introduce variable activation energy Q and σ_b into the parabolic growth law. Afterwards, Chen et al. [14] derived a thermo-kinetic model for the evolution of grain size by incorporation of the reduced GB energy into the parabolic kinetics of grain growth. Furthermore, a thermo-kinetic description was performed by Gong et al. [17] for nanoscale grain growth through analysis of the effect of GB segregation on the initial GB excess amount, Γ_b. However, the initial GB condition and corresponding controlled-mechanism of thermal stability in NC Fe–B alloys has not still been reported.

This paper presented a formation of single-phase supersaturated nanograins prepared by melt spinning technique in low-solid-solubility Fe–B alloys. Combining the effect of GB segregation on the initial GB excess amount, the thermo-kinetic model

* Corresponding author at: School of Material Science and Engineering, China University of Mining and Technology, Xuzhou, Jiangsu 221008, PR China. Tel.: +86 0516 83897715; fax: +86 0516 83591870.
E-mail address: chenzheng1218@163.com (Z. Chen).

0925-8388/$ – see front matter.
doi:10.1016/j.jallcom.2011.08.051

considering the mixed effects of solute drag and reduced GB energy was extended to describe the initial GB condition of NC Fe–B alloys. On this basis, the initial GB condition of NC Fe–B alloys was determined. Finally, based on two characteristic annealing times (t_1 and t_2), the controlled-mechanism of grain size evolution was discussed.

2. Experimental details

NC Fe–B ribbons were prepared using melt spinning technique. High-purity elemental Fe and B better than 99.9% were mixed to form 3 g Fe–B master alloy containing 8, 10, 12 and 14 at.% B, respectively. The master alloy was melted with the temperature up to 1300 K (≈100 K superheat) in a quartz tube under the protection of Ar atmosphere. Under a pressure of 150 mbar, the melt in the tube was ejected through a slotted nozzle (i.d. ≈0.9 mm) onto a rotating Cu wheel (diameter D_{Cu} = 200 mm); a small gap of about 0.7 mm was held between the nozzle and the Cu wheel. The cooling rate was controlled through the variation of the melt puddle size by changing the tangential speed of Cu wheel (21–73 m/s). The detailed experimental processes and parameters could be found in Ref. [8].

To investigate the behavior of NC grain growth and solute segregation, isothermal annealing at 700 °C were conducted in a vacuum electric resistance furnace under the protection of Ar atmosphere at different annealing times.

X-ray diffraction (XRD) was performed for the as-spun and as-annealed samples on a Panalytical X'pert Pro type X-ray diffractometer with Cu Kα radiation (λ_{Cu} = 0.1542 nm) at a slow scan rate of 0.01 s^{-1} and 100 steps per degree. The contributions of Cu Kα were subtracted out using XRD software (MDI Jade 5.0) and the instrumental broadening was removed using a Si-powder standard. The average value of the grain sizes was calculated using the Scherrer formula from five intense peaks (1 1 0, 2 0 0, 2 1 1, 2 2 0, 3 1 0), with the standard deviation of these values from the above peaks as the error. Several annealing experiments were repeated and XRD analysis was performed to check the reproducibility of the experimental results.

The as-spun and as-annealed microstructures and crystallography characteristics of the spun Fe–B ribbons were studied using JEM-200CK transmission electron microscopy (TEM) and selected-area electron diffraction (SAED). The structures and sizes evidenced by XRD were validated further by TEM.

3. Experimental results

Applying melt spinning technique, single-phase supersaturated nanograins were prepared for low-solid-solubility Fe–B alloys. However, the as-spun single-phase nanograins were unstable. Upon annealing at high temperatures, grain growth occurred with segregation of B atoms to GBs.

3.1. Formation of single-phase supersaturated nanograins

Generally, the equilibrium microstructures at room temperature (RT) for the hypoeutectic Fe–B alloys are α-Fe and α-Fe + Fe_2B [18]. However, upon melt spinning the cooling rate is several orders larger than that of the equilibrium solidification, which leads to the kinetic undercooling much higher than the hypercooling limitation of the alloy melt. Accordingly, an irregular eutectic morphology (α-Fe + Fe_3B) was formed under the hypercooled state instead of the equilibrium hypoeutectic structure [19].

Fe–10 at.% B alloy was taken as an example to analyze the formation of single-phase supersaturated nanograins in the melt spinning process. In order to prepare nanograins in Fe–10 at.% B alloy, the precipitation (i.e., Fe_2B or Fe_3B) caused by solute segregation must be suppressed. Fig. 1 shows the XRD profile of samples prepared at different tangential speeds of Cu wheel (m/s). For 21 m/s, both α-Fe and Fe_2B phases were observed. It could be confirmed further by TEM in Fig. 2, which showed eutectic morphology (α-Fe + Fe_2B). To identify each phase in the as-solidified structure, SAED analyses were also performed (see Fig. 2b and c), which showed that the white area belonged to α-Fe phase and the dark area belonged to Fe_2B phase. But the content of Fe_2B phase decreased and almost vanished with the increase of tangential speed of Cu wheel as shown in Fig. 1. For 73 m/s, only α-Fe phase was found in the melt-spun sample (Fig. 3), which was consistent with the corresponding XRD profile (i.e., without Fe_2B or metastable Fe_3B phase) as shown in Fig. 1.

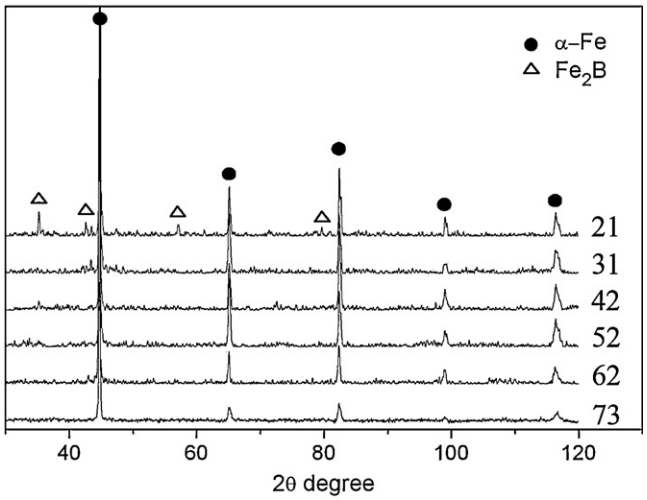

Fig. 1. XRD pattern for the melt spun Fe–10 at.% B alloy with different tangential speeds of Cu wheel (m/s).

The other essential condition of forming the single-phase supersaturated nanograins is that the grain size in the as-spun samples must reduce to the nanoscale. Because of the higher cooling rate the grain size of Fe–B alloys reduced to nanoscale rapidly. This can be evidenced by the XRD pattern shown in Fig. 1 and TEM results shown in Fig. 3.

Until now, the single-phase supersaturated nanograins have been prepared in Fe–10 at.% B alloy. Similar results could also be obtained in the samples of Fe–8 at.% B, Fe–12 at.% B, Fe–14 at.% B alloys (Fig. 1). Afterwards isothermal annealing of the as-spun single-phase supersaturated nanograins at 700 °C was conducted.

3.2. Heat treatment of the as-spun nanograins

Fig. 4 shows bright-field TEM images of the Fe–10 at.% B samples annealed for 1 h and 1.5 h at 700 °C, respectively. The XRD spectra of NC Fe–B ribbons containing 8, 10, 12 and 14 at.% B annealed at 700 °C for different annealing times are plotted in Fig. 5, where only α-Fe phase is identified. XRD profile confirmed that no other phases were present in any of the annealed samples. The grain size determined by XRD is plotted in Fig. 6. In comparison of the grain size determined by TEM, it is confirmed that the average grain size determined by XRD is proper. As shown in Fig. 6, obvious grain growth occurred with the annealing time and then tended to a stabilized value.

It should be noted that the solute segregation of B cannot be observed from Fig. 4. Herein the thermo-kinetic grain growth model was employed to analyze the process of grain growth and the effect of solute segregation of B (see Sections 5.2 and 6.2). The detection of solute segregation will be performed in our coming work directly.

4. Thermo-kinetic grain growth models applicable for NC Fe–B alloys

4.1. Kinetic model

The driving force for GB migration arises from its curvature. A classical theory for grain growth from Burke and Turnbull [20] deduces that the growth rate, V (i.e., dD/dt) is related to the interface mobility, M, and the driving force $P(V)$,

$$V = MP(V) = M\frac{\sigma_b}{D} \Rightarrow \frac{1}{M}\frac{dD}{dt} = \frac{\sigma_b}{D} \quad (1)$$

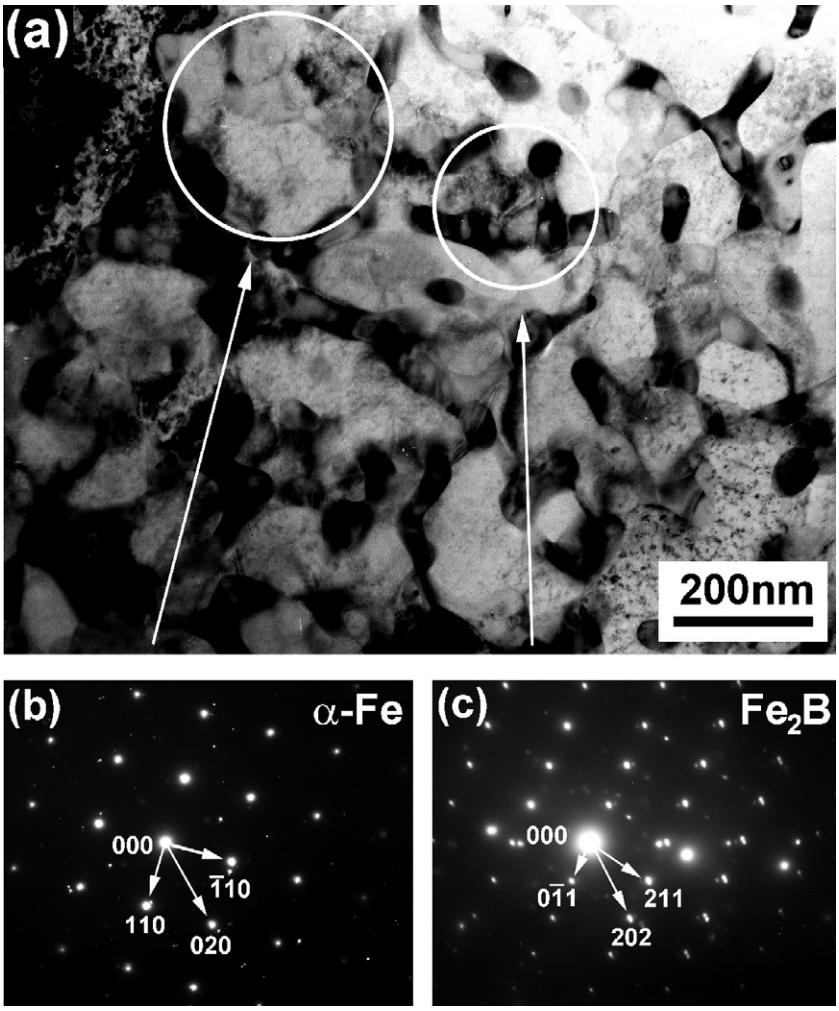

Fig. 2. Typical bright field morphology of the melt-spun Fe–10 at.% B alloy with the tangential speed of 21 m/s: (a) microscopic morphology, (b) SAEDP of α-Fe and (c) SAEDP of Fe_2B.

This classical parabolic model is precisely applicable to high-purity, single-phase materials. In general, both M and $P(V)$ are functions of state variables such as T and x_0 [21]. As for NC solutions, the solute drag term P_S is introduced to model the stagnation of growth in most real materials. Regarding the dependence of solute drag on GB concentration (X_{GB}) and V, the drag term should be given as $P_S = \beta D \times dD/dt$ [22], so that the driving force is revised as,

$$P(V) = P_S + \frac{V}{M} \Rightarrow \left(\frac{1}{M} + \beta D\right)\frac{dD}{dt} = \frac{\sigma_b}{D} \quad (2)$$

with β as a constant. As compared to the previous model from Michels et al. [11], an integrated effect of solute drag due to X_{GB} and V is thus expected as a more rational manner for the stabilization [23].

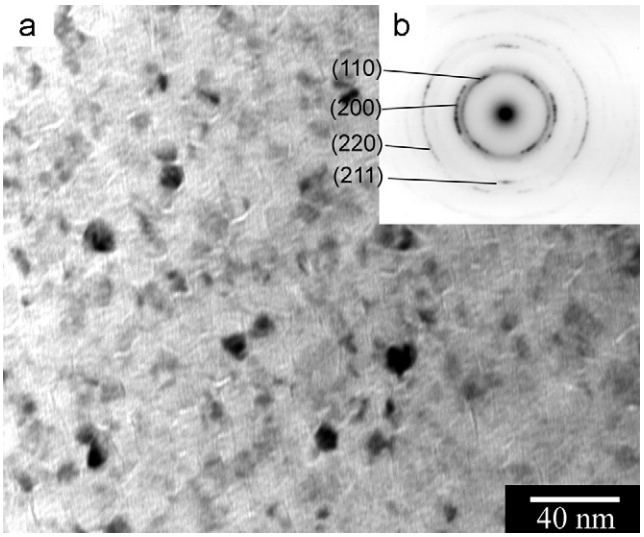

Fig. 3. Typical bright field morphology (a) and diffraction spot (b) of the melt spun Fe–10 at.% B nanograins with tangential speed of 73 m/s.

4.2. Thermodynamic model

In 1992, Weissmüller [24] first presented a concept for the stabilization of NC solids against grain growth by GB segregation. Later, an analogous analytical treatment was derived by Kirchheim [12] and Liu et al. [13] on the basis of Gibbs adsorption equation [25],

$$\sigma_b = \sigma_0 - \Gamma_{b0}\left[\mathrm{RT}\ \ln\left(x_0 - \frac{3\Gamma_b V_m}{D}\right) + \Delta H_{seg}\right] \quad (3)$$

where σ_0 is the GB energy for pure solvent, V_m the molar volume of the alloy, ΔH_{seg} the enthalpy change of segregation per mole of solute, x_0 the average concentration of the whole system, Γ_{b0} the saturated solute excess amount, Γ_b ($\leq \Gamma_{b0}$) is the solute excess amount at GBs.

It can be inferred from Eq. (3) that grain growth stops with Γ_b approaching Γ_{b0} as σ_b is close to zero. However, is the GB segre-

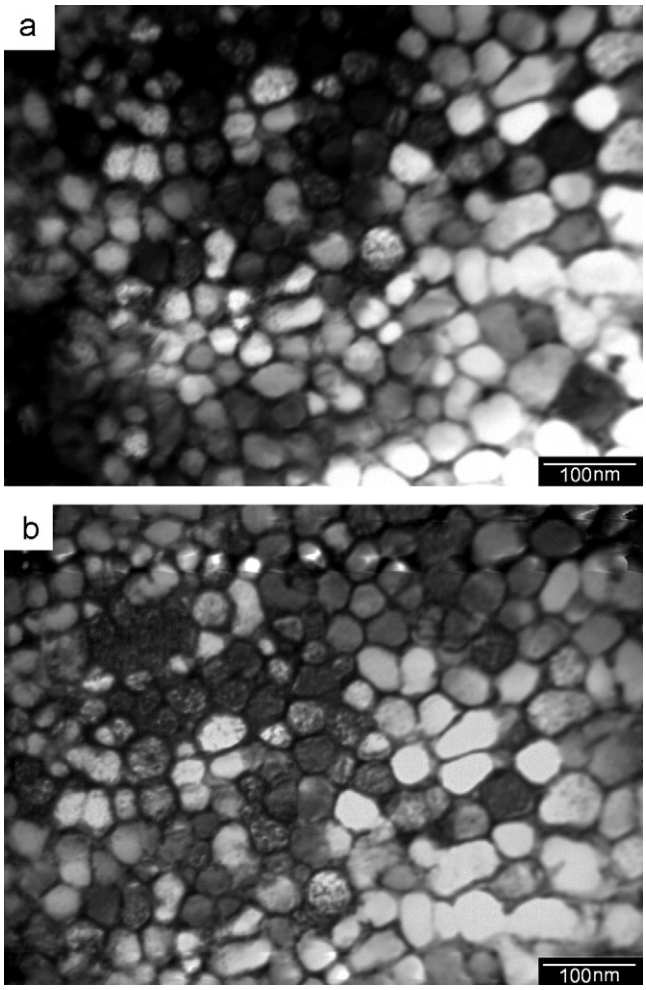

Fig. 4. Bright field TEM images for the melt spun Fe–10 at.% B nanograins (73 m/s) annealed at 700 °C for 1 *h* (a) and 1.5 *h* (b), respectively.

gation saturated or not at the beginning of grain growth, i.e., the value of Γ_b must be lower than or equal to Γ_{b0}? Departing from Gibbs equation [25] and McLean's treatment for GB segregation [26], Gong et al. [17] categorized the state criterion of initial GB segregation as saturated GB segregation condition ($\Gamma_b/\Gamma_{b0} = 1$) and unsaturated GB segregation condition ($\Gamma_b/\Gamma_{b0} < 1$).

For $\Gamma_b/\Gamma_{b0} = 1$, according to the first order Taylor expansion, Eq. (3) can be rewritten as,

$$\sigma_b = \sigma_0 - \Gamma_{b0}(\mathrm{RT}\ \ln x_0 + \Delta H_{\mathrm{seg}}) + \frac{3\mathrm{RT}\Gamma_{b0}^2 V_m}{x_0}\frac{1}{D} \tag{4}$$

For $\Gamma_b/\Gamma_{b0} < 1$, Eq. (3) can be rewritten as,

$$\sigma_b = \sigma_0 - \Gamma_{b0}(\mathrm{RT}\ \ln x_0 + \Delta H_{\mathrm{seg}}) + \frac{3\Gamma_{b0}\mathrm{RT}\,V_m\Gamma_b}{x_0 D} \tag{5}$$

Applying the equation of mass conservation to strongly segregating systems, the GB excess for NC materials is obtained as [14],

$$\Gamma_b = \delta(\rho_{\mathrm{GB}}X_{\mathrm{GB}} - \rho_g X_g) \approx x_0\rho\left(\frac{D}{6} + \delta\right) \tag{6}$$

with δ as the GB thickness, ρ_{GB} and ρ_g as the density, and X_{GB} and X_g as the concentration, of the GB and the matrix.

Substitution of Eq. (6) into Eq. (5) leads to,

$$\sigma_b = \sigma_0 - \Gamma_{b0}\left[\mathrm{RT}\left(\ln\ x_0 - \frac{V_m\rho}{2}\right) + \Delta H_{\mathrm{seg}}\right] + 3\Gamma_{b0}\mathrm{RT}\ V_m\delta\rho\frac{1}{D} \tag{7}$$

Apparently, Eq. (7) is analogous to $\sigma_b = \sigma_1 - \sigma_2 D$ from Chen et al. [14] and the difference between Eq. (7) and that from Chen et al. lies in whether the effect of the configurational entropy is considered or not.

4.3. Thermo-kinetic model

With reference to [14,27], as the GB area decreases upon grain growth, the segregated solute atoms must be re-distributed throughout the GB network. Meanwhile, the activation energy for GB diffusion is increased, accompanied with a decreased GB diffusion coefficient, D_b. From Borisov's equation [27], once D_b and the lattice diffusion coefficient D_l become equivalent, a thermodynamic metastable equilibrium state (i.e., $\sigma_b = 0$) results. Thus, incorporation of the GB energy decreasing with GB segregation into the parabolic kinetics is physically practicable [28]. Analogous to the treatment of Ref. [14], a substitution of Eq. (5) and Eq. (7) into Eq. (2) leads to,

$$\int_{D_0}^{D}\frac{D(1/M + \beta D)}{\sigma_1 + (\sigma_2/D)}dD = \int_0^t dt \tag{8}$$

with

$$\begin{aligned}\sigma_1 &= \begin{cases}\sigma_0 - \Gamma_{b0}\left[\mathrm{RT}(\ln x_0 - \frac{V_m\rho}{2}) + \Delta H_{\mathrm{seg}}\right], & \frac{\Gamma_b}{\Gamma_{b0}} < 1,\\ \sigma_0 - \Gamma_{b0}[\mathrm{RT}(\ln x_0) + \Delta H_{\mathrm{seg}}], & \frac{\Gamma_b}{\Gamma_{b0}} = 1,\end{cases}\\ \sigma_2 &= \begin{cases}3\Gamma_{b0}\,\mathrm{RT}\,V_m\delta\rho, & \frac{\Gamma_b}{\Gamma_{b0}} < 1,\\ \frac{3\Gamma_{b0}^2\,\mathrm{RT}\,V_m}{x_0} & \frac{\Gamma_b}{\Gamma_{b0}} = 1\end{cases}\end{aligned} \tag{9}$$

and the boundary condition as: $t = 0$, $D = D_0$ and $t = t$, $D = D(t)$.

Integrating Eq. (8) leads to an evolution of grain size with time,

$$\begin{aligned}&\left\{\frac{\beta}{3\sigma_1}\left[\left(D + \frac{\sigma_2}{\sigma_1}\right)^3 - \left(D_0 + \frac{\sigma_2}{\sigma_1}\right)^3\right] + \left(\frac{1}{2\sigma_1 M} - \frac{3}{2}\frac{\beta\sigma_2}{\sigma_1^2}\right)\right.\\ &\times\left[\left(D + \frac{\sigma_2}{\sigma_1}\right)^2 - \left(D_0 + \frac{\sigma_2}{\sigma_1}\right)^2\right] + \left(\frac{3\beta\sigma_2^2}{\sigma_1^3} - \frac{2\sigma_2}{M\sigma_1^2}\right)(D - D_0)\\ &\left.+\left(\frac{\sigma_2^2}{\sigma_1^3 M} - \frac{\beta\sigma_2^3}{\sigma_1^4}\right)\ln\frac{D + (\sigma_2/\sigma_2)}{D_0 + (\sigma_2/\sigma_1)}\right\} = t\end{aligned} \tag{10}$$

with D_0 as the initial average grain size. Eq. (10) is defined as the model for grain growth considering the mixed effect due to kinetics and thermodynamics. The equation gives the evolution of the average grain size with the annealing time.

5. Model applications

The as-spun nanograins were not the final stabilized microstructure. Upon annealing at high temperatures, grain growth occurred.

5.1. Validity of the thermo-kinetic model

Because of the intrinsic limitation of thermodynamic and kinetic models, the present model is a relative intact one in that it couples the mixed effects due to thermodynamics and kinetics for the analysis of nanoscale grain growth in Fe–B alloys. Subjected to specific limitations, Eq. (10) will be reduced to previous models.

1. **Pure thermodynamic and pure kinetic limitations:** (i) if the GB energy effect is neglected (σ_b is considered as an average, constant GB energy), Eq. (10) will be reduced to Rabkin's model [23] (pure kinetic model, Eq. (2)); (ii) If the kinetic process

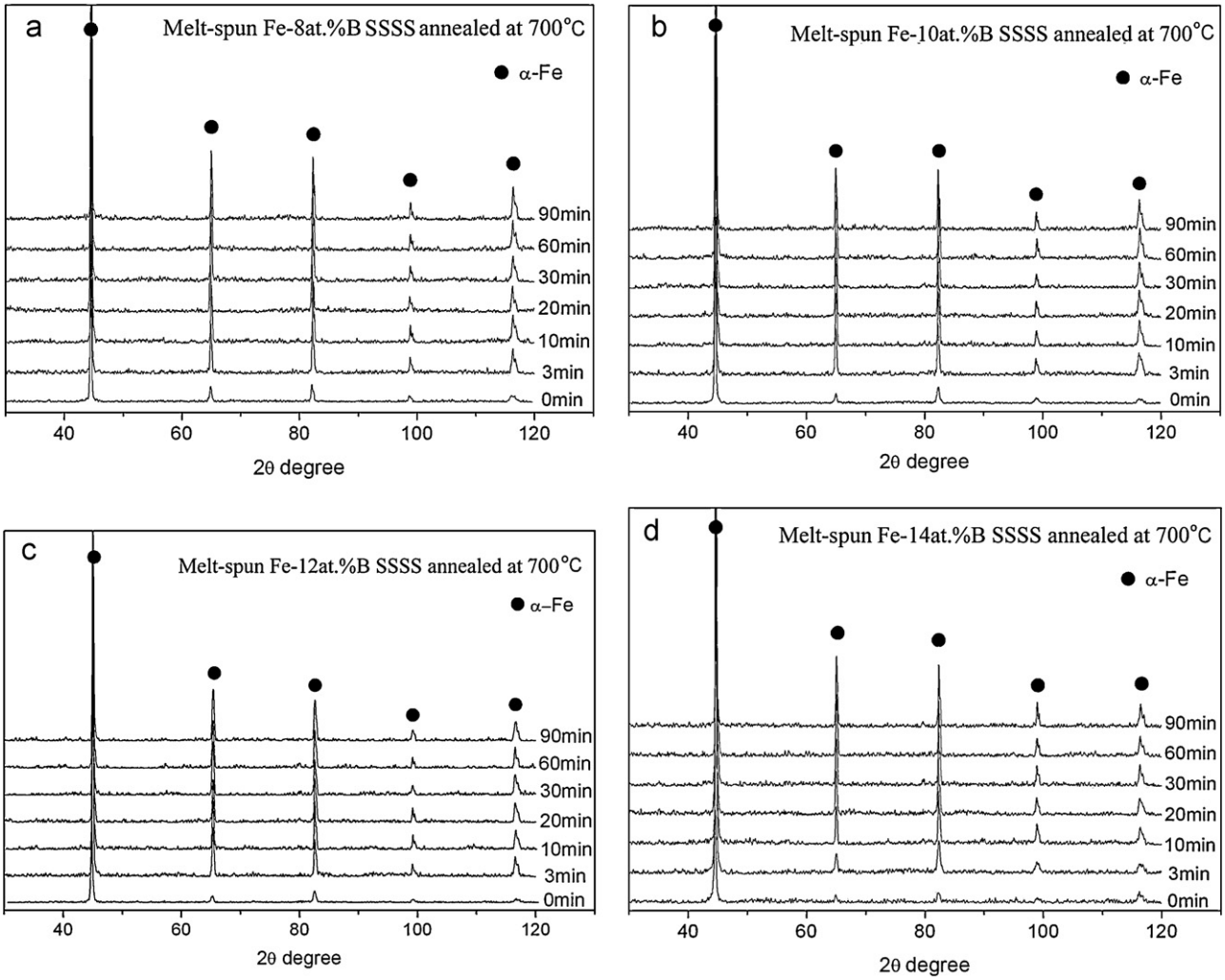

Fig. 5. XRD patterns for the melt spun Fe–B alloys (73 m/s) annealed at 700 °C for different times: (a) Fe–8 at.% B, (b) Fe–10 at.% B, (c) Fe–12 at.% B and (d) Fe–14 at.% B.

is neglected, Eq. (10) will be reduced to pure thermodynamic model (Eqs. (5) and (7)) which is consistent with the illustration by Kirchheim's [12].

2. **Initial GB condition limitations:** (i) if $\Gamma_b/\Gamma_{b0} < 1$, Eq. (10) will be reduced to Chen et al.'s model (a thermo-kinetic analytical model at unsaturated GB condition [14]); (ii) if $\Gamma_b/\Gamma_{b0} = 1$ and the solute drag effect is neglected, Eq. (10) will be reduced to Gong et al's model (a thermo-kinetic analytical model at saturated GB condition [17]).

5.2. Model calculations

The Fe–B system has an equilibrium solubility limit of 0.04 at.% B in Fe at 890 °C and the equilibrium solubility is reduced further to near zero at lower temperatures [18]. Therefore, the thermo-kinetic model is quite applicable for describing nanograin growth in melt spun Fe–B alloys with strong segregating tendency. The parabolic model (Eq. (1)), pure kinetic model (Eq. (2)), pure thermodynamic model (Eqs. (4) and (7)) and thermo-kinetic model (Eq. (10)) are applied to analysis the mechanism of grain growth.

As shown in Fig. 6, the parabolic model (Eq. (1) with constant σ_b and $\beta = 0$), the pure kinetic model (Eq. (2) with σ_b as constant and $\beta = 1/MD_0$ [23]) and the thermo-kinetic model (Eq. (10)) with $\beta = 1/M$[1]) were applied to fit the experimental data employing the parameters listed in Table 1. From Fig. 6a, the classical parabolic model (dotted lines) cannot be brought into agreement with the experimental data. The pure kinetic model could fit the initial stage within 1000 s. Although the rate of grain growth is partially inhibited due to the solute drag effect, the pure kinetic model could not give a satisfied description. A good fit to the experimental data is only obtained using the present thermo-kinetic model (Eq. (10)) due to the introduction of the mixed effect of GB energy and solute drag.

In the fit of Eq. (10) to the experimental data, σ_0 was 0.83 J/m^2 according to the analysis of Darling et al. for NC Fe-based alloys [29] while Γ_{b0}, M and ΔH_{seg} acted as the fitting parameters; see a detailed fitting procedure given in Ref. [14]. As for different initial GB conditions (i.e., $\Gamma_b/\Gamma_{b0} < 1$ and $\Gamma_b/\Gamma_{b0} = 1$), the fitted values of Γ_{b0} and M were almost uniform (Table 1). When $\Gamma_b/\Gamma_{b0} < 1$, ΔH_{seg} was fitted as 70.84, 69.23, 67.94 and 66.81 kJ/mol; when $\Gamma_b/\Gamma_{b0} = 1$, ΔH_{seg} was fitted as 67.04, 65.45, 64.11 and 62.88 kJ/mol

[1] The selection of constant β will not influence the model analysis. For example, $\beta = \sigma_b/D_{max}^2$ (with D_{max} as the limiting grain size) was determined by Michels [11]; Rabkin [23] gave a hypothetical value $\beta = 1/MD_0$. Regarding the complexity of calculation depending on β, $\beta = \sigma_2/M$ was assumed by Chen et al. [14]. In order to derive an analytical model, $\beta = 1/M$ was assumed in the present case.

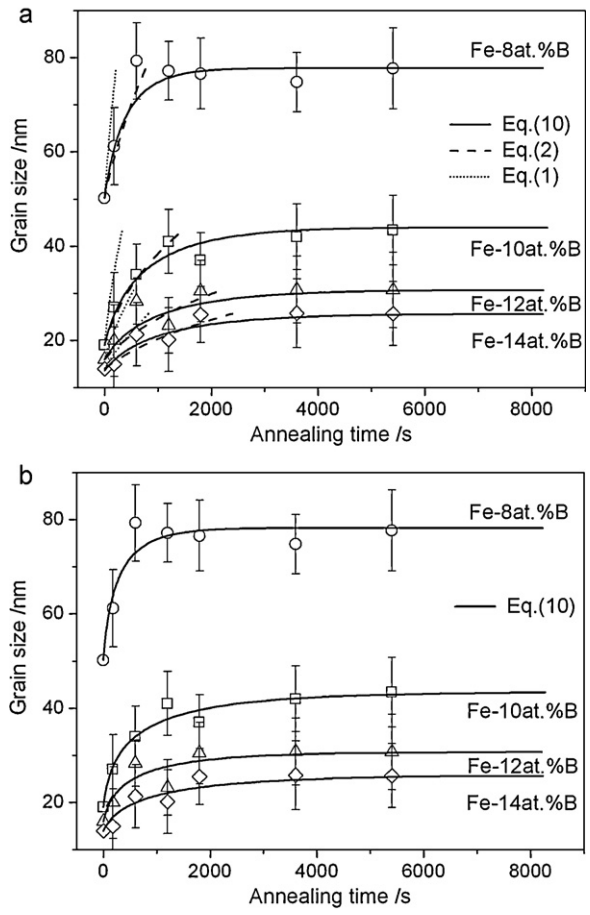

Fig. 6. Evolution of the average grain size with the annealing time for the melt-spun Fe–B nanograins (73 m/s) annealed at 700 °C. The symbols are the experimental data with different B concentrations. (a) The dotted, dashed, solid lines are calculated using Eq. (1) (the parabolic model), Eq. (2) (the pure kinetic model) and Eq. (10) (the present thermo-kinetic model at $\Gamma_b/\Gamma_{b0} = 1$), respectively; (b) the solid line is calculated using Eq. (10) at $\Gamma_b/\Gamma_{b0} < 1$.

(Table 1) for alloys with 8, 10, 12 and 14 at.% B, respectively. ΔH_{seg} was roughly estimated as 75.63 kJ/mol using the equation of $\Delta H_{seg} \approx RT \ln x_{op} - (10 \pm 6)$ with x_{op} (≈0.04 at.% B in Fe at $T \approx 890$ °C [18]) as the terminal solute solubility [12], which is compatible with the fitted values of the two cases.

According to the analysis of Section 4.3, the thermo-kinetic model was classified two cases, i.e., the initial saturated GB condition and the initial unsaturated GB condition. As shown in Fig. 6a and b, both of models could give fit descriptions. That is to say, the thermo-kinetic model is applicable for describing the process of grain growth and as for the NC Fe–B alloys the initial GB condition should be analyzed further (see Section 6.1).

6. Discussion

In Section 3, the formation of the as-spun single-phase supersaturated nanograins and the subsequent grain growth and solute segregation were described for melt spun Fe–B alloys. It is evidenced that the grains grew rapidly during a relatively short period of time and then the grain size did not change essentially any more with time. Based on the present thermo-kinetic model, the initial GB condition and possible controlled-mechanism of grain growth will be discussed in this part.

6.1. Analysis of initial GB condition

According to the analysis of Section 5.2, it is still difficult to determine the initial GB condition of grain growth in NC Fe–B alloys. In addition, both the thermo-kinetic models at saturated condition and unsaturated condition could give satisfied description. It means that it is difficult to determine the actual initial GB condition through the comparison of the fitting parameters, Γ_{b0}, M and ΔH_{seg} (Section 5.2).

According to the analysis of Gong et al. [17], the initial GB condition could be decided by the ratio of Γ_b/Γ_{b0}. If $\Gamma_b/\Gamma_{b0} \approx 1$, it is a saturated GB condition; And if $\Gamma_b/\Gamma_{b0} \ll 1$, it is an unsaturated GB condition. A combination of McLean's treatment of GB segregation [26] and the two relations $X_g = x_0 - \Gamma_b V_m/D$ (where X_g is the concentration of the matrix, Eq. (3)) [12] and $\Gamma_b \approx \delta\rho X_{GB}$ (Eq. (6)) [30] leads to the relation [17],

$$\frac{\Gamma_b}{\Gamma_{b0}} \approx \left[1 + \frac{\exp(-(\Delta H_{seg}/RT))}{x_0 - (3\Gamma_b V_m/D)}\right]^{-1} \quad (11)$$

In combination of the calculated results of Eq. (10) at $\Gamma_b/\Gamma_{b0} < 1$ and the parameters in Table 1, the evolution of Γ_b/Γ_{b0} with the annealing time is calculated and shown in Fig. 7, where Γ_b/Γ_{b0} (0.995–0.996) approaches 1. It is evidenced that the initial saturated GB condition is determined in NC Fe–B alloys. Conceptually, the GB energy is reduced with segregation since solute atoms can effectively reduce elastic mismatch strains in the GBs [31]. As for Fe–B alloys, the large B solute concentration (8–12 at.%) and the extreme low-solid-solubility of B in Fe (≈0.04 at.% B in Fe at $T \approx 890$ °C [18]) implied extensive GB segregation for these systems. This result was also evidenced in NC Ni–O sample with 6039 ppm O [32], where Γ_b/Γ_{b0} was calculated as 0.9948 and 0.9998 by Gong et al. [17]. Similarly, due to the strong segregating tendency and high solute concentration in NC Fe–B alloys, the initial saturated GB condition ($\Gamma_b/\Gamma_{b0} \approx 1$) was determined.

6.2. Characteristic time and controlled-mechanism of grain growth in NC Fe–B alloy

As described in Refs. [14,15,28], grain growth is a kinetic process controlled by thermodynamic factor. That is to say, the thermodynamic factor or kinetic factor may play the main role at

Table 1
Values for physical parameters of NC Fe–B alloys used in the calculations in terms of Eq. (10).

Parameters	Concentration (at.%)			
	8	10	12	14
GB energy, σ_0 (J/m^2)	0.83	0.83	0.83	0.83
Saturated excess, Γ_{b0} (at.%)	1.8×10^{-5}	1.8×10^{-5}	1.8×10^{-5}	1.8×10^{-5}
Actual GB thickness, δ (nm)	0.8	0.8	0.8	0.8
Enthalpy change, ΔH_{seg} (kJ/mol) ($\Gamma_b/\Gamma_{b0} = 1$)	67.04	65.45	64.11	62.88
Enthalpy change, ΔH_{seg} (kJ/mol) ($\Gamma_b/\Gamma_{b0} < 1$)	70.84	69.23	67.94	66.81
Mobility, M ($\times$m^4/J s) ($\Gamma_b/\Gamma_{b0} = 1$)	3.9×10^{-15}	3.5×10^{-16}	1.3×10^{-16}	5.9×10^{-17}
Mobility, M (m^4/J s) ($\Gamma_b/\Gamma_{b0} < 1$)	6.1×10^{-15}	3.9×10^{-16}	1.6×10^{-16}	5.9×10^{-17}

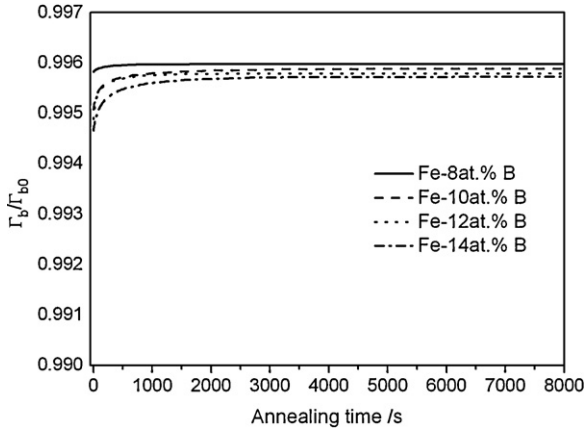

Fig. 7. Evolution of Γ_b/Γ_{b0} with the annealing time for the melt-spun Fe–B nanograins (73 m/s) annealed at 700 °C. It is calculated by Eq. (11) in combination of Eq. (10) at $\Gamma_b/\Gamma_{b0} < 1$ using parameters in Table 1.

different periods in the whole annealing process. Obviously, the rapid increase of grain size is a kinetic process (Fig. 6), and the final period is a thermodynamic stabilized stage. Three theoretical models of grain growth (pure kinetic model (Eq. (2)), pure thermodynamic model (Eq. (4)) and thermo-kinetic model (Eq. (10)) were compared in Fig. 8. Both Eqs. (2) and (10) could describe the rapid increase of grain size well at the period of $t \le t_1$. It can be concluded that the evolution of grain size was controlled by the same mechanism (i.e., mainly kinetic-controlled mechanism) at $t \le t_1$. However, the grain size D_{kinetic} determined by Eq. (2) increased continuously and exceeded the grain size $D_{\text{thermo-kinetic}}$ determined by Eq. (10) at $t > t_1$ as shown in Fig. 8. It indicated that the controlled-mechanism of grain growth happened to change from kinetic-controlled mechanism to mixed mechanism of kinetics and thermodynamics at t_1 because of the incorporation of GB energy effect. Therefore, t_1 could be determined as an important characteristic time.

On the other hand, as shown in Fig. 8, both Eq. (4) ($\sigma_b = 0$) and Eq. (10) could describe the stabilized grain size at the period of $t \ge t_2$ well. As shown in Fig. 8, $D_{\text{thermo-kinetic}}$ tended to D^* because of the GB energy effect and almost reached it at t_2 ($\sigma_b = 0$). Therefore, t_2 could be determined as another characteristic time which forecasted a transition from mixed controlled growth to purely thermodynamic-controlled growth.

From above analysis, in comparison of Eqs. (2), (4) and (10), two critical annealing times were defined,

$$t = \begin{cases} t_1, & D_{\text{kinetic}} = D_{\text{thermo-kinetic}} \\ t_2, & D \approx D^*(\sigma_b \approx 0) \end{cases} \quad (12)$$

With regard to the two characteristic times, the controlled-mechanism can be categorized as follows:

(i) Mainly kinetic-controlled growth ($t \le t_1$):

Using the parameters listed in Table 1, the evolution of GB energy with the annealing time is calculated according to Appendix A and shown in Fig. 8. At $t \le t_1$, GB energy as the driving force of GB migration is of a higher value. On the other hand, the comparison of Eqs. (1), (2) and (10) shows that solute drag effect is not able to inhibit grain growth. The resistance of GB migration induced by solute drag is feeble, thus grain grows rapidly at the initial stage. Therefore, it is a mainly kinetic controlled-mechanism at the range of $t \le t_1$.

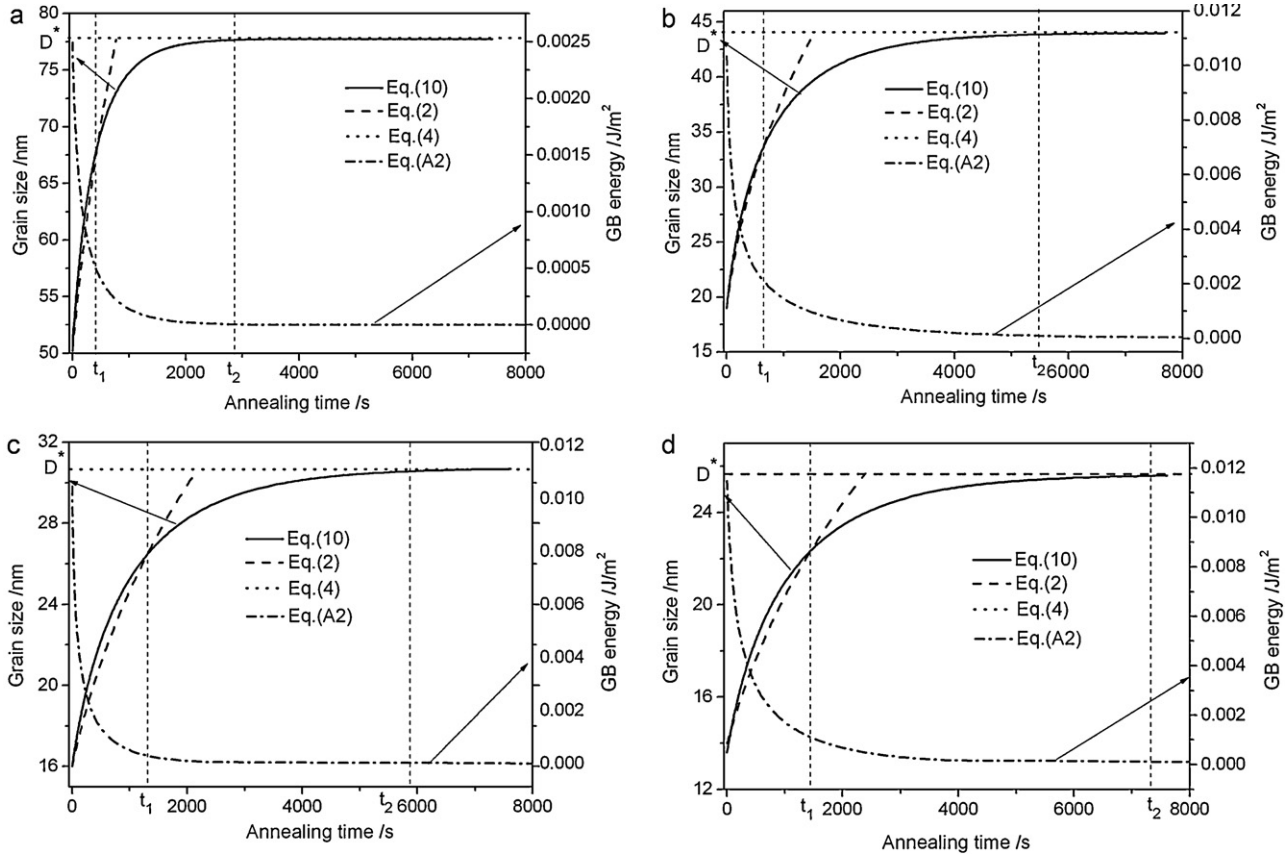

Fig. 8. Evolution of the average grain size and GB energy with the annealing time for the melt-spun Fe–B nanograins (73 m/s; 8, 10, 12 and 14 at.% B) annealed at 700 °C. GB energy is calculated using Eq. (A2). Two critical annealing times were determined. t_1: D_{kinetic} determined by Eq. (2) equals to $D_{\text{thermo-kinetic}}$ determined by Eq. (10); t_2: $D_{\text{thermo-kinetic}}$ tends to D^* when σ_b tends to 0 (D^* is determined using Eq. (4) when $\sigma_b = 0$).

(ii) A transition from kinetic-controlled growth to thermodynamic-controlled growth ($t_1 < t < t_2$):

As shown in Fig. 8, the grain size $D_{\text{thermo-kinetic}}$ determined by Eq. (10) increased slowly because of the introduction of GB effect and was exceeded by the grain size D_{kinetic} determined by Eq. (2) at $t > t_1$. As for the low-solid-solubility Fe–B alloys, the effect of thermodynamics increased with solute segregation (Fig. 8). Therefore, at the range of $t_1 < t < t_2$, it is a transition of the controlled-mechanism from main kinetic mechanism to main thermodynamic mechanism.

(iii) Pure thermodynamic-controlled growth ($t \geq t_2$):

Apparently, only rapid increase of grain size occurs at $t \leq t_1$. Once $t \geq t_2$, $\sigma_b \sim 0$, the stabilized size D^* was calculated using Eq. (4) (see Fig. 8),

$$D^* = \frac{3\Gamma_{b0}^2\ \mathrm{RT}\, V_m/x_0}{\Gamma_{b0}(\mathrm{RT}\ln x_0 + \Delta H_{\text{seg}}) - \sigma_0} \tag{13}$$

Therefore, with the decrease of driving force of GB migration, the thermodynamic effect is a key stabilized mechanism at the final stage in melt spun Fe–B alloys.

Thermodynamical equilibrium GB segregation is considered in the whole theoretical treatment using the present thermo-kinetic model. Equilibrium GB segregation occurs as a result of inhomogeneities in the solid giving rise to sites of GBs for which solute atoms have a lower free energy [33]. In real grain growth of nanograins in Fe–B alloys, the initial condition, i.e., the distribution of solute atoms between grain interior and GBs may not be thermodynamical equilibrium, and thus some time is needed for solute atoms to diffuse into GBs to reach equilibrium. The analogous phenomenon was evidenced in Ni–P experiment [34] that the stagnation of grain growth was due to P solute segregation [14]. Similar results were also found in NC Pd–Zr and Fe–Zr alloys [21,35].

7. Conclusions

A grain growth process in the melt spun low-solid-solubility Fe–B alloys was analyzed under the initial saturated GB segregation condition. Applying melt spinning, single-phase supersaturated nanograins were prepared. Grain growth behavior of the single-phase supersaturated nanograins was investigated by performing isothermal annealings at 700 °C. The main conclusions of this analysis can be summarized as follows:

1. In combination with the effect of GB segregation on the initial GB excess amount, the thermo-kinetic model was extended to describe the initial grain boundary condition of NC Fe–B alloys.
2. In comparison of pure kinetic model, pure thermodynamic model and the extended thermo-kinetic model, an initial saturated GB segregation condition was determined.
3. The characteristic times (t_1 and t_2) were determined. The controlled-mechanism of grain growth in NC Fe–B alloys was proposed, including a mainly kinetic-controlled process ($t \leq t_1$), a transition from kinetic-mechanism to thermodynamic-mechanism ($t_1 < t < t_2$) and pure thermodynamic-controlled process ($t \geq t_2$).

Acknowledgements

The authors are grateful to the Natural Science Foundation of China (Grant no. 51101169), the Fundamental Research Funds for the Central Universities (2010QNA06) and the fund of the State Key Laboratory of Solidification Processing in NWPU (SKLSP201119).

Appendix A. Calculation of the GB energy with annealing time

A quasi-quantitative analysis for the effect of GB energy on the grain growth is given by differentiation of Eq. (4) over t,

$$\frac{d\sigma_b}{dt} = \frac{\sigma_2}{D^2}\frac{dD}{dt} \tag{A1}$$

In combination with Eqs. (4) and (A1) with $\beta = 1/M$ (see Section 5.2) leads to,

$$\int_{\sigma_1}^{\sigma_b} \frac{\sigma_1 + \sigma_2 - \sigma_b}{(\sigma_1 - \sigma_b)^4 \sigma_b} d\sigma_b = \frac{M}{\sigma_2^2}\int_0^t dt \tag{A2}$$

The evolution of GB energy with the annealing time for as-spun Fe–B nanograins was calculated (Fig. 8) using the parameters listed in Table 1. As shown in Fig. 8, σ_b decreases with grain growth, but it approaches only infinitely zero (Fig. 8). Thermodynamically, "zero" value should be considered as an ideally limitation for σ_b [16].

References

[1] T. Nagase, A. Yokoyama, Y. Umakoshi, J. Alloys Compd. 509 (2011) 1178–1186.
[2] Y.H. Zhang, B.W. Li, H.P. Ren, X. Ding, X.G. Liu, L. Chen, J. Alloys Compd. 509 (2011) 2808–2814.
[3] Y. Wu, M.V. Lototsky, J.K. Solberg, V.A. Yartys, J. Alloys Compd. (2010), doi:10.1016/j.jallcom.2010. 11.140.
[4] X.F. Miao, Y.G. Wang, M. Guo, J. Alloys Compd. 509 (2011) 2789–2792.
[5] G. Herzer, Nanomagnetism, Kluwer Academic Publishers, Dordrecht, 1993, p. 111.
[6] Y.F. Liu, Y.H. Cao, L. Huang, M.X. Gao, H.G. Pan, J. Alloys Compd. 509 (2011) 675–686.
[7] Z.W. Chen, Y.M. Lei, H.F. Zhang, J. Alloys Compd. 509 (2011) 7473–7477.
[8] Z. Chen, F. Liu, K. Zhang, Y.Z. Ma, G.C. Yang, Y.H. Zhou, J. Cryst. Growth 313 (2010) 81–89.
[9] Z. Huda, T. Zaharinie, J. Alloys Compd. 478 (2009) 128–132.
[10] J.E. Burke, Trans. Metall. Soc. AIME 175 (1949) 73–91.
[11] A. Michels, C.E. Krill, H. Ehrhardt, R. Birringer, D.T. Wu, Acta Mater. 47 (1999) 2143–2152.
[12] R. Kirchheim, Acta Mater. 50 (2002) 413–419.
[13] F. Liu, R. Kirchheim, J. Cryst. Growth 264 (2004) 385–391.
[14] Z. Chen, F. Liu, H.F. Wang, W. Yang, G.C. Yang, Y.H. Zhou, Acta Mater. 57 (5) (2009) 1466–1475.
[15] K. Zhang, Z. Chen, F. Liu, G.C. Yang, J. Alloys Compd. 501 (2010) L4–L7.
[16] F. Liu, R. Kirchheim, Thin Solid Films 466 (2004) 108–113.
[17] M.M. Gong, F. Liu, K. Zhang, Scr. Mater. 63 (2010) 989–992.
[18] H. Okamoto, Phase Diagrams of Binary Iron Alloys, ASM International, Materials Park, OH, 1993, pp. 41–47, 131–137.
[19] C.L. Yang, F. Liu, S.T. Ren, G.C. Yang, J. Magn. Magn. Mater. 321 (2009) 91–94.
[20] J.E. Burke, D. Turnbull, Prog. Met. Phys. 3 (1952) 220–292.
[21] C.E. Krill, H. Ehrhardt, R. Birringer, Z. Metallkd. 96 (2005) 1134–1141.
[22] J.W. Cahn, Acta Metall. 10 (1962) 789–798.
[23] E. Rabkin, Scr. Mater. 42 (2000) 1199–1206.
[24] J. Weissmüller, Nanostruct. Mater. 3 (1993) 261–272.
[25] J.W. Gibbs, Trans. Conn. Acad. III 108 (1876);
J.W. Gibbs, Trans. Conn. Acad. III 343 (1878);
J.W. Gibbs, The Collected Works of J.W. Gibbs, vol. 1, Longmans, Green and Co, New York, 1928, pp. 55–354.
[26] D. Mclean, Grain Boundaries in Metals, Oxford University Press, Oxford, 1957.
[27] V.T. Borisov, V.M. Golikov, G.V. Scherbedinskiy, Fiz. Met. Metalloved. 17 (1964) 80–85.
[28] X. Song, J. Zhang, L. Li, K. Yang, G. Liu, Acta Mater. 54 (2006) 5541–5550.
[29] K.A. Darling, B.K. VanLeeuwen, J.E. Semones, C.C. Koch, R.O. Scattergood, L.J. Kecskes, S.N. Mathaudhu, Mater. Sci. Eng. A 528 (2011) 4365–4371.
[30] G. Gottstein, L.S. Shvindlerman, Grain Boundary Migration in Metals, Thermodynamics, Kinetics, Applications, CRC Press, 1999.
[31] M.P. Seah, J. Phys. 10 (1980) 1043–1046.
[32] H. Natter, M.S. Löffler, C.E. Krill, R. Hempelmann, Scr. Mater. 44 (2001) 2321–2325.
[33] T.D. Xu, B.Y. Cheng, Prog. Mater. Sci. 49 (2004) 109–208.
[34] B. Färber, E. Cadel, A. Menand, G. Schmitz, R. Kirchheim, Acta Mater. 48 (2000) 789–796.
[35] K.A. Darling, R.N. Chan, P.Z. Wong, J.E. Semones, R.O. Scattergood, C.C. Koch, Scr. Mater. 59 (2008) 530–533.